



ORIGINAL RESEARCH ARTICLE

# Preparation and Characterization of Ni60-WC Composites Fabricated Using Laser Cladding Technique

Chunyang Ma, Huaxing Li, Fafeng Xia, and Peng Yan

Submitted: 29 December 2023 / Revised: 19 February 2024 / Accepted: 27 February 2024

**In order to improve the surface properties of metal knives, agricultural appliances, and other metal parts, Ni60-WC composites were fabricated by using laser cladding (LCG) technique. The impacts of WC addition on the surface and cross-sectional morphologies, Vickers hardness, phase structure, corrosion resistance, and wear resistance of the composites were investigated. The findings suggested that WC particles had a significant impact on the structural characteristics of the Ni60-WC composites. Cross sections of Ni60-WC10 and Ni60-WC20 composites revealed the presence of numerous elements, including Ni, W, C, Fe, and Cr, confirming that the LCG approach could effectively fabricate Ni60-WC composites. Furthermore, numerous nickel grains and WC particles emerged in Ni60-WC20 composites, and the average nickel grain and WC particle diameters were reported as 96.3 and 54.6  $\mu\text{m}$ , respectively. The Ni60-WC20 composite showed an average Vickers hardness of 826.9 HV, which was around 3.5 times higher than the Vickers hardness of the substrate. Similarly, the Ni60-WC20 composite demonstrated excellent anti-wear resistance. Additionally, the Ni60-WC20 composite demonstrated remarkable corrosion resistance, as reflected by its corrosion potential measurement of only  $-0.37$  V.**

**Keywords** laser cladding, morphology, Ni60-WC composite, preparation, WC addition, wear resistance

## 1. Introduction

Generally, the Ni60 composites exhibit several exceptional features, such as high hardness and remarkable resistance to wear and corrosion. Consequently, they have found extensive applications in enhancing the properties of metallic components and technique appliances (Ref 1, 2). Nevertheless, the composite material has a slightly reduced durability in comparison to alternative materials as a result of its vulnerability to the development of cracks, porosity, and other imperfections during the laser cladding (LCG) procedure. As a result, several researchers have tried to incorporate ceramic particles (such as TiC, TiN, SiC, and WC) into nickel-based composites. Chen et al. (Ref 3) investigated the impact of including TiC and TiN on the structural characteristics and wear behavior of Ni-TiC-TiN composites. The successful production of Ni-TiC composites with exceptional mechanical characteristics was reported by Ma et al. (Ref 4) through the LCG approach. Ni-WC composites were studied for their structural characteristics and corrosion behavior by Farahmand et al. (Ref 5). The incorporation of WC and Mo particles was found to improve the nickel

grains. The corrosion and thermal fatigue characteristics of Ni60-TiC composites generated using the electroless plating process were investigated by Pan et al. (Ref 6). They discovered that Ni60-TiC composites could enhance the quality of coating preparation.

WC ceramic particles have been proverbially known for their application in metalwork, chemical industry, and agricultural machinery for their outstanding performances (Ref 7). Conventionally, to augment the property, specifically in relation to surface hardness, wear resistance, and anti-corrosion property, WC micro-/nano-particles are strategically incorporated into metal composites to refine metal grains and enhance the performance of the composites. As a result, metal-based WC composites have arose as a new area of extensive discussion during the past few years (Ref 8-10). Wang et al. (Ref 11) successfully prepared Ni-WC gradient composites by using laser cladding technique. Ma et al. (Ref 12) reported that Ni60/WC composites could be fabricated by using wide-band laser cladding. They found that the wear resistance of coatings was promoted to 6.8 times that of substrate. Wang et al. (Ref 13) studied the mechanisms on heat damage of WC particles in Ni60/WC composites, and manufactured Ni60/WC composites via laser induction hybrid cladding technique. While many studies have focused on the synthesis and analysis of nickel-based composites, few have investigated how the addition of WC affects the composite's structure and properties when utilizing the LCG method of preparation. Therefore, it is crucial to conduct a comprehensive examination of the influence of WC content on the structural and mechanical characteristics of Ni60-WC composites. The present study employed the LCG approach for the fabrication of Ni60 and Ni60-WC composites. In addition, the microhardness apparatus, x-ray diffractometer (XRD), scanning electron microscope (SEM), stereoscopic microscope, electrochemical workstation, and friction and wear tester were employed to examine the impact of WC particles on

**Chunyang Ma, Huaxing Li, and Fafeng Xia**, College of Engineering, Northeast Agricultural University, Harbin 150030, China; and **Peng Yan**, College of Engineering, Northeast Agricultural University, Harbin 150030, China; and College of Mechanical Science and Engineering, Northeast Petroleum University, Daqing 163318, China. Contact e-mails: chunyangandma@163.com and xiaff@neau.edu.cn.

the structures and characteristics of LCG-ed Ni60-WC composites.

## 2. Experimental Procedure

In this study, a total of 45 steel samples measuring  $250 \times 150 \times 30$  mm were utilized as the substrates. Due to its extensive utilization in the production of mechanical components, agricultural appliances, and chemical containers, 45 steel gained significant importance (Ref 14-16). The Ni60 powders and WC particles were obtained from Harbin Zhuoyuan Nano-materials Co. Ltd. The average diameters of the Ni60 powders and WC particles were estimated to be around 50 and 35  $\mu\text{m}$ , respectively. Before the implementation of LCG, a YXQM-8 ball grinder (Changsha Miqi Equipment Co., Ltd.) was employed to uniformly mix Ni60 powders and WC particles, maintaining a mass ratio of 10% for WC and 20% for Ni powders. The rotary speed was set at 120 r/min, and the mixing time was set to 5 h.

An LM-2000WA laser melting machine (Wuhan Lishui Laser Technology Co., Ltd.) was employed for producing Ni60 and Ni60-WC composites. The LCG method was performed using argon as the carrier gas, which was introduced through two nozzles positioned beneath the samples. The pressure of the argon gas was maintained at 0.2 MPa. The laser power was consistently maintained at 1.5 kW, the rate at which the sample was traversed was 1000 mm/min, and the beam diameter and the degree of overlap between tracks were 3 mm and 50%, respectively. Following the LCG process, the surfaces of Ni60 and Ni60-WC composites underwent polishing using 800 and 1000# abrasive papers, followed by a thorough cleaning with acetone and distilled water. The Ni60-WC composites deposited at mass ratios of 10 and 20%, respectively, were designated as Ni60-WC10 and Ni60-WC20.

The elemental distribution, surface, and cross-sectional morphologies of Ni60 and Ni60-WC composites were examined using a SEM (S3400, Hitachi Ltd.). Electron backscatter diffraction (EBSD) analysis was also performed to observe crystallographic orientations and WC distribution. The composites' phase structures were examined with a D/MAX-2400 type XRD instrument (Rigaku Corporation). The radiation utilized in the experiment was  $\text{CuK}\alpha$ , while the voltage applied to the accelerating tube was 30 kV. The scanning step and range were set at  $0.04^\circ/\text{s}$  and  $10 \sim 90^\circ$ , respectively. The Vickers hardness values of Ni60 and Ni60-WC composites were studied using a DHV-1000 Vickers hardness tester (Shanghai Precision Instrument Co., Ltd.). The testing parameters included an applied load of 10 N and a dwelling duration of 15s. Utilizing a GWT-3G wear machine (Jinan Hengxu Testing Machine Technology Co., Ltd.) with a 3 mm GCr15 steel ball, the anti-wear properties of Ni60 and Ni60-WC composites were analyzed. The wear rate was set to 150 r/min, while the load applied and wear time was 100 N and 30 min, respectively. An S3400 SEM and an ESM-120 stereoscopic microscope (Qiangdao Shanyi Instrument Co., Ltd.) were employed to examine the worn microstructures of Ni60 and Ni60-WC composites. In addition, the corrosion characteristics of Ni60 and Ni60-WC composites were assessed in a 3.5wt.% NaCl corrosion solution for 48 h, employing a CHI-600E electrochemical workstation (Shanghai Chenhua Instrument Co., Ltd.). The corrosion weight losses ( $\Delta M$ ) of Ni60 and Ni60-WC composites were

measured by using a ZA200R3 type electronic analytical balance (Shanghai Zanwei Technology Co., Ltd.) with a precision of 0.1 mg. The corrosion rates ( $v$ ) of the composites can be calculated by using Eq 1.

$$v = \Delta M / (S \times t) \quad (\text{Eq 1})$$

where  $S$  is the area of the composite ( $\text{m}^2$ ), and  $t$  is the corrosion time (h).

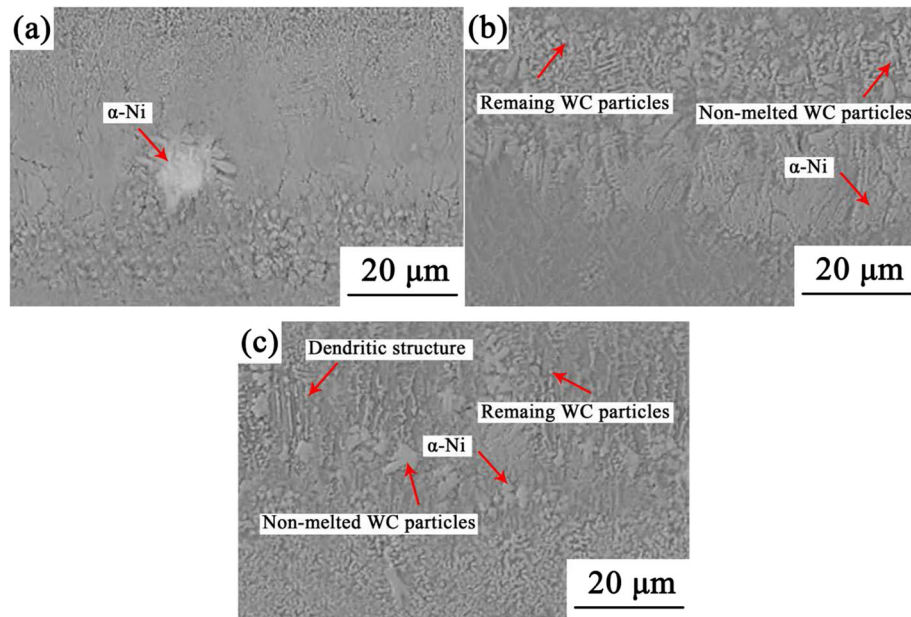
## 3. Results and Discussion

### 3.1 Influence of WC Addition on the Composite Morphologies

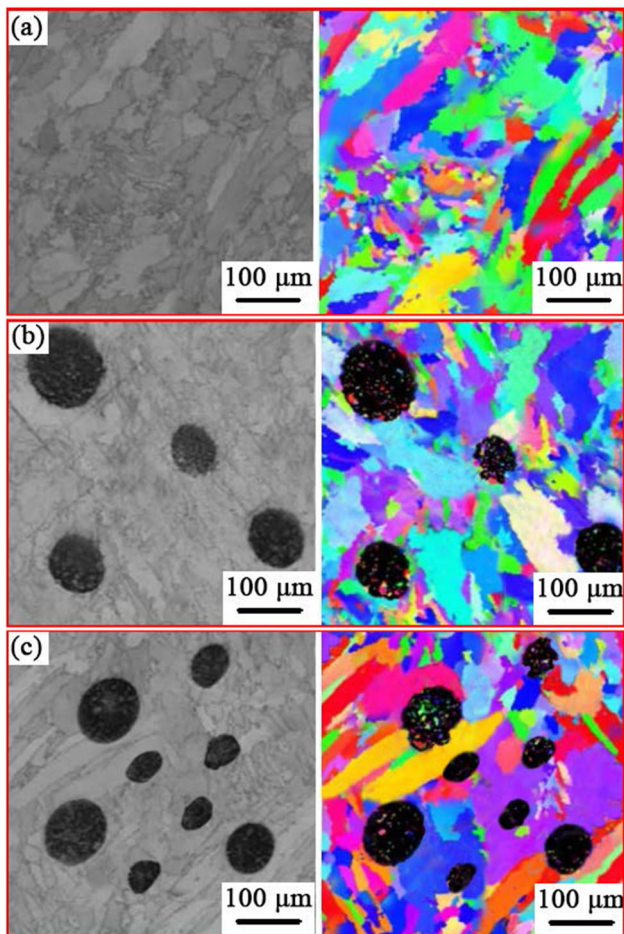
Figure 1 depicts the influence of WC content on the surface morphologies of Ni60 and Ni60-WC composites. It was determined that none of the three composites exhibited any cracks. The surface of the Ni60 composite exhibited the presence of several  $\alpha$ -Ni phases, characterized by a substantial and coarse microstructure (Fig. 1a). In comparison to the Ni60 composite, the Ni60-WC10 composite had a fine and compact structure with larger gray-white dendritic tissues. In addition, several unmelted WC nanoparticles were discovered on the composite's surface. In contrast, as shown in Fig. 1(c), the Ni60-WC20 composite had the most uniform and dense microstructure of the three coatings. Similarly, several small-sized WC particles were observed on the Ni60-WC20 composite.

This phenomenon can be elucidated by the following explanation: (1) The presence of ceramic particles within composites has been found to have a substantial impact on both the nucleation and development of metal grains (Ref 17-21). In comparison to the Ni60 composite, Ni60-WC composites contain a greater number of WC particles, which provides numerous nucleation sites for the metal grains, leading to a notable reduction in the growth of Ni grains. Thus, the structures of the Ni60-WC10 and Ni60-WC20 composites were more refined than those of the Ni60 composite. (2) The addition of WC particles had a substantial effect on the composite's structure (Ref 5, 22). The Ni-WC composite exhibited a notable fine-crystal reinforcing (FCR) effect due to the higher WC addition in the Ni60-WC20 composite compared to the Ni60-WC10 composite (Ref 23, 24). Thus, the Ni60-WC20 composite had a finer and more compact microstructure than the Ni60-WC10 composite.

Figure 2 reveals the EBSD results of Ni60 and Ni60-WC composites along the cladding direction. Remarkably, not a single WC particle was present in the Ni60 composite (Fig. 2a). Many large nickel grains appeared in the composite. The average grain diameter was approximately 138.2  $\mu\text{m}$ . Nevertheless, an astonishingly small amount of WC particles were triumphantly embedded into the Ni60-WC10 composite (Fig. 2b). It was noteworthy that the introduction of WC had refined the metal grains in Ni60-WC composites. The average nickel grain and WC particle diameters were about 112.7 and 72.4  $\mu\text{m}$ , respectively. Moreover, an abundance of WC particles with columnar structures were embedded within the Ni60-WC20 composite (Fig. 2c). Furthermore, numerous nickel grains and WC particles emerged in Ni60-WC20 composites, and the average nickel grain and WC particle diameters were reported as 96.3 and 54.6  $\mu\text{m}$ , respectively.



**Fig. 1** SEM images of (a) Ni60 composite, (b) Ni60-WC10 composite and (c) Ni60-WC20 composite.



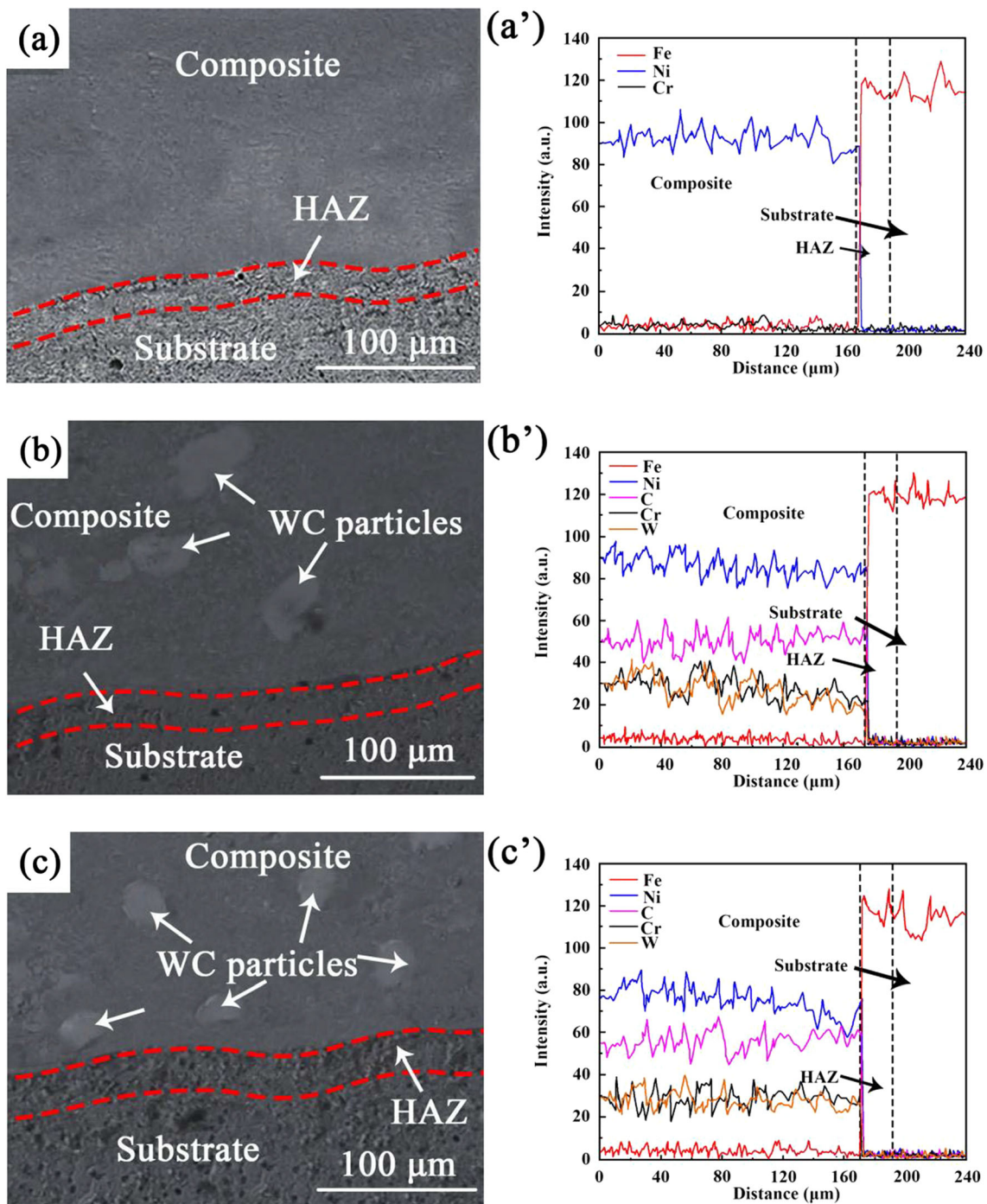
**Fig. 2** EBSD results of (a) Ni60 composite, (b) Ni60-WC10 composite and (c) Ni60-WC20 composite.

Figure 3 depicts element scanning curves and cross-sectional images of Ni60, Ni60-WC10, and Ni60-WC20

composites. In the three composites, there was no discernible boundary between the substrate and the composite. Additionally, the heat-affected zone (HAZ) yielded numerous refined metal grains (Ref 25-28). The Ni60 composite had numerous Ni elements, as illustrated in Fig. 3(a) and (a'). Due to the presence of Fe and Cr in the original Ni60 powders, only a small number of these elements appeared in the composite. However, the cross-sectional analysis of Ni60-WC10 and Ni60-WC20 composites revealed the presence of numerous elements such as Ni, W, C, Fe, and Cr, hence confirming the effective utilization of the LCG method in the prefabrication of Ni60-WC composites (Ref 29-31). W and C additions were found to be greater in the Ni60-WC20 composite than in the Ni60-WC10 composite, owing to the addition of twice as many WC particles in the Ni60-WC20 composite. This increased the FCR effect on the Ni60-WC20 composite, leading to the composite's most refined and compact microstructure.

### 3.2 Effect of WC Addition on the XRD Spectra of Ni60-WC Composites

Figure 4 depicts XRD phase analyses of Ni60, Ni60-WC10, and Ni60-WC20 composites. The Ni60 composite exhibited the presence of  $\gamma$ -(Ni,Fe) and  $\text{Ni}_3\text{Fe}$  phases, with diffraction peaks observed at 43.6, 50.1, and 74.7°, respectively. The present finding aligns with the literature as reported by Liu et al. (Ref 5). Ni60-WC10 and Ni60-WC20 composites, on the other hand, showed abundant  $\gamma$ -(Ni,Fe),  $\text{W}_2\text{C}$ , WC,  $\text{M}_7\text{C}_3$ ,  $\text{M}_{23}\text{C}_6$ , and  $\text{Ni}_3\text{Fe}$  phases, which is evidence of the successful implantation of WC particles. Furthermore, in comparison to the other composites, the Ni60-WC20 composite displayed the weakest and broadest diffraction peaks for  $\text{Ni}_3\text{Fe}$  and  $\gamma$ -(Ni,Fe) and grains, suggesting the development of a fine and compact structure. Compared to other composites, the Ni60 composite exhibited high and narrow diffraction peaks of  $\text{Ni}_3\text{Fe}$  and  $\gamma$ -(Ni,Fe) grains, signifying a coarse and massive microstructure.

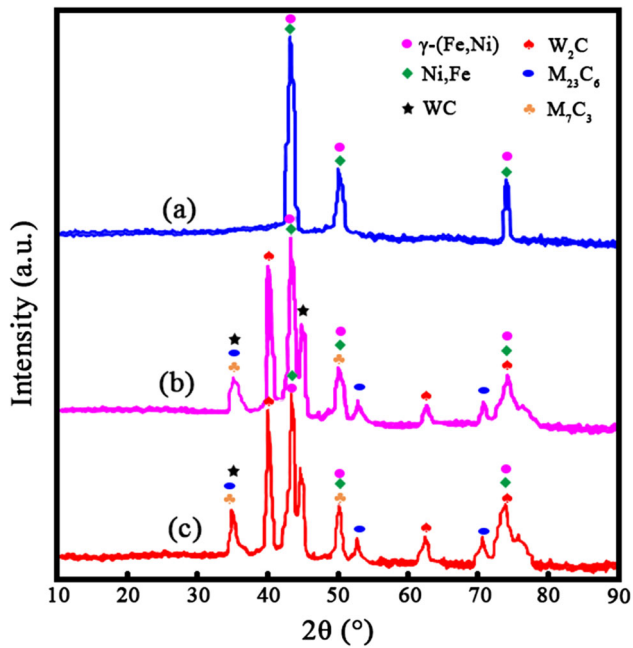


**Fig. 3** Cross-sectional images and element scanning curves of Ni60-WC composites: (a) and (a') Ni60 composite, (b) and (b') Ni60-WC10 composite, (c) and (c') Ni60-WC20 composite.

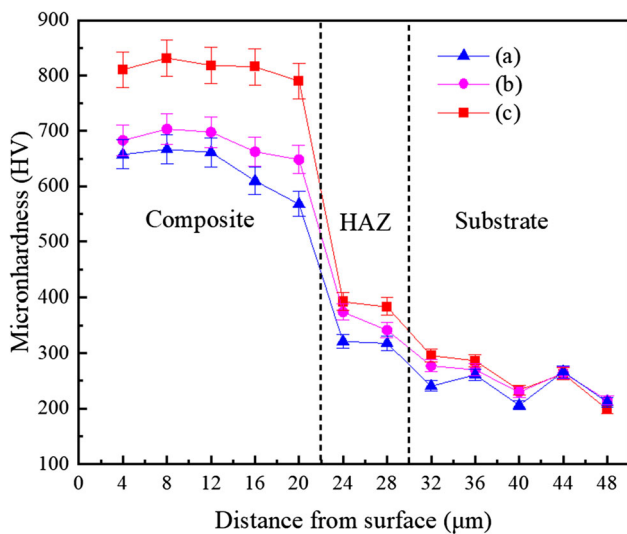
### 3.3 Influence of WC Addition on the Composite Hardness

Figure 5 presents the Vickers hardness values of Ni60, Ni60-WC10, and Ni60-WC20 composites. The findings indicate that the average Vickers hardness of the Ni60-WC20 composite material was found to be roughly 3.5 times greater than the substrate material ( $\sim 247.2$  HV). This significant

increase in hardness can be due to the presence of hard phases, including  $M_7C_3$ ,  $Ni_3Fe$ ,  $M_{23}C_6$ , and WC, which were formed during the LCG process. The aforementioned finding is supported by the hardness data presented in Fig. 6, which indicates that the WC particles exhibited a hardness of around 1300 HV (Ref 32, 33). However, the average hardness values of Ni60 and Ni60-WC10 composites were determined to be



**Fig. 4** X-ray diffraction patterns of (a) Ni60 composite, (b) Ni60-WC10 composite and (c) Ni60-WC20 composite.



**Fig. 5** Microhardness dataset of (a) Ni60 composite, (b) Ni60-WC10 composite and (c) Ni60-WC20 composite.

605.1 HV and 651.8 HV, respectively. The production of fine metal grains during the LCG process is responsible for the higher microhardness of the HAZ compared to the substrate (Fig. 5).

### 3.4 Effect of WC Addition on Anti-wear Behaviors of Ni60-WC Composites

Figure 7 depicts the 2D, 3D worn images and wear depths of LCG-fabricated Ni60, Ni60-WC10, and Ni60-WC20 composites. During the wear test, notable wear grooves of significant

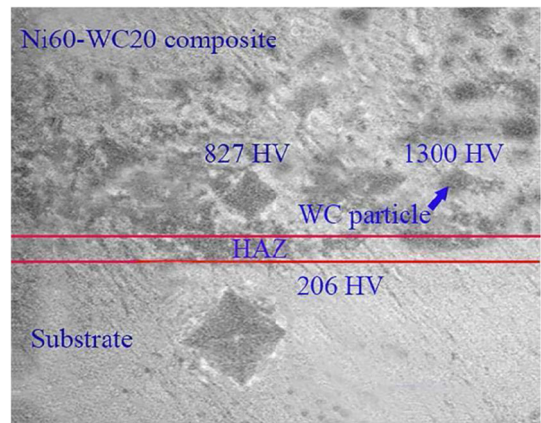


**Fig. 6** Indentation image of Ni60-WC20 composite.

depth and width were observed on the surface of the Ni60 composite. The wear depth was measured to be around  $26.6 \mu\text{m}$ , suggesting substantial wear of the Ni60 composite (Fig. 7a, a' and a"). Adding WC particles to Ni60-WC composites significantly augmented their anti-wear capabilities. This was achieved by embedding WC particles within Ni60, helping restrain the growth of Ni grains and refine those within the composite. In particular, the Ni60-WC20 composite demonstrated exceptional resistance to wear. On the worn surface of the Ni60-WC20 composite, only a few shallow grooves were observed with a wear depth of approximately  $5.9 \mu\text{m}$  (Fig. 7c, c', and c"). The enhancement in the anti-wear resistance of the Ni60-WC20 composite was shown to be directly correlated with the incorporation of WC particles (Ref 34). The incorporation of WC particles into the Ni60-WC composite as a reinforcing phase resulted in notable enhancements in both composite hardness and coating wear resistance. Furthermore, throughout the wear experiment, it was observed that as the metal grains of the Ni60-WC composite underwent wear, the WC particles that were exposed during the process transformed into grinding grains. This transformation resulted in a shift in the wear mechanism from sliding friction to rolling friction, hence providing resistance against external friction forces on the composite (Ref 35). In addition, the compact/fine structure of the Ni60-WC20 composite allowed it to withstand the friction ball's wear, thereby exhibiting an exceptional anti-wear property.

Figure 8 depicts the friction coefficients of LCG-fabricated Ni60, Ni60-WC10, and Ni60-WC20 composites. The friction coefficients of Ni60, Ni60-WC10, and Ni60-WC20 composites exhibited a rapid increase as the duration of wear shifted from 0 to 120s, indicating that the three coatings were undergoing the initial stage of wear. The friction coefficient values did not change significantly after the wear time exceeded 120s. Importantly, the Ni60 composite displayed the highest friction coefficient of 0.58 among all composites. This can be attributed to its coarse and large grain structure (Ref 36, 37). However, the friction coefficients for Ni60-WC10 and Ni60-WC20 composites were 0.49 and 0.41, respectively.

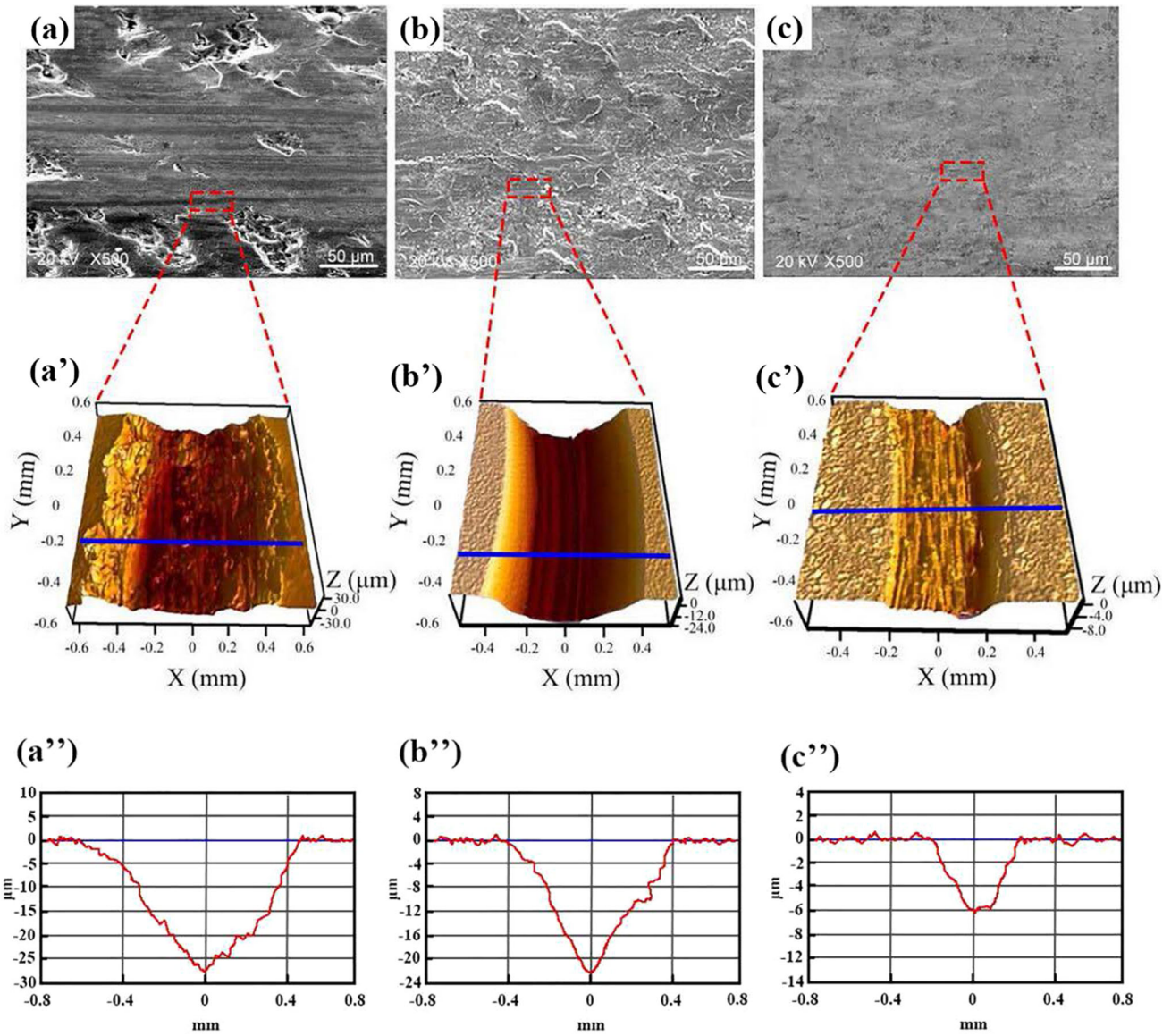


**Fig. 7** 2D, 3D worn morphologies and wear depths of (a), (a') and (a'') Ni60 composite, (b), (b') and (b'') Ni60-WC10 composite and (c), (c') and (c'') Ni60-WC20 composite.

### 3.5 Effect of WC Addition on Anti-corrosion Behaviors of Ni60-WC Composites

Figure 9 displays the polarization curves of Ni60, Ni60-WC10, and Ni60-WC20 composites. The corrosion potential of the Ni60-WC20 composite material was determined to be  $-0.37$  V, which suggests a comparatively lower value in comparison to both the Ni60 and Ni60-WC10 composites. This finding suggests that the Ni60-WC20 composite exhibits

exceptional resistance to corrosion. However, the corrosion potential value of the Ni60 composite was  $-0.84$  V, indicating weak corrosion resistance. In addition, corrosion current densities of Ni60, Ni60-WC10 and Ni60-WC20 composites were  $9.6 \times 10^{-5}$ ,  $8.1 \times 10^{-5}$ , and  $5.4 \times 10^{-5}$  A/cm<sup>2</sup>, respectively.

To investigate the corrosion characteristics of Ni60 and Ni60-WC composites, three samples were prepared with

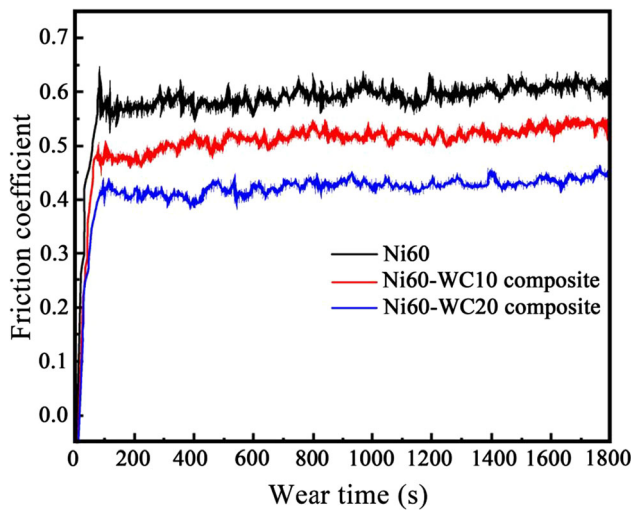


**Fig. 8** Friction coefficients of Ni60, Ni60-WC10 and Ni60-WC20 composites.

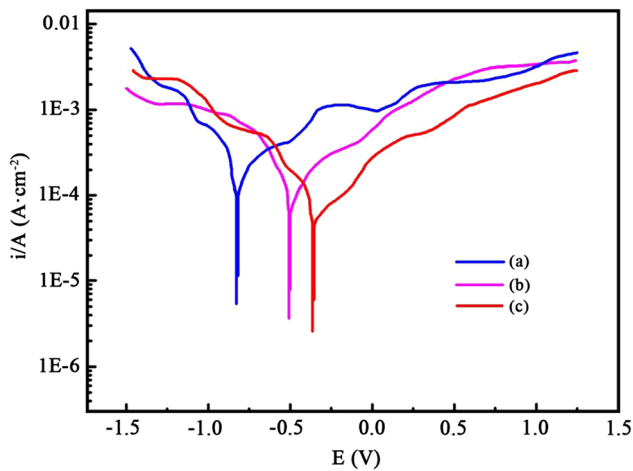


**Fig. 9** Polarization curves of (a) Ni60 composite, (b) Ni60-WC10 composite and (c) Ni60-WC20 composite.

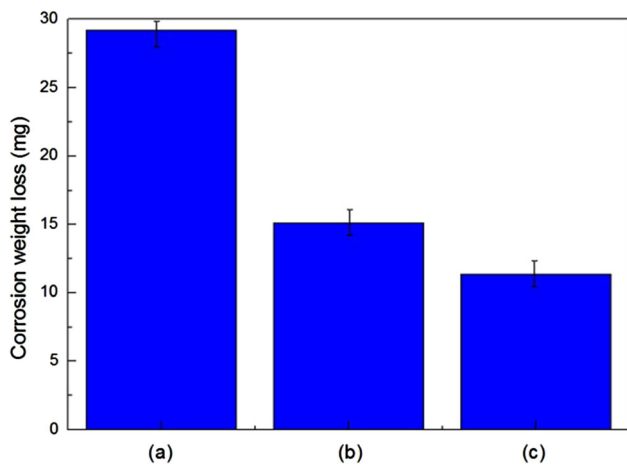


**Fig. 10** The corrosion weight losses of Ni60 and Ni60-WC composites after 48 h of corrosion experiments: (a) Ni60 composite, (b) Ni60-WC10 composite and (c) Ni60-WC20 composite.

coatings of Ni60, Ni60-WC10, and Ni60-WC20. Subsequently, the samples were immersed in a corrosive liquid containing 3.5wt.% NaCl for 48 hours. The  $\Delta M$  values of Ni60 and Ni60-WC composites are displayed in Fig. 10. According to Eq 1, the corrosion rates of Ni60, Ni60-WC10, and Ni60-WC20 composites were 16.22, 8.39, and 6.33  $\text{mg}/(\text{m}^2\cdot\text{h})$ , respectively. The SEM corrosion morphologies of Ni60 and Ni60-WC composites are depicted in Fig. 11. The enhanced contact area between the grain and the corrosion solution is considerably facilitated by the existence of a coarse and loose structure in the Ni60 composite, as depicted in Fig. 9(a). Consequently, this facilitates the incorporation of NaCl liquid into the composite, increasing corrosion mass (Ref 38-41). Therefore, the Ni60 composite demonstrated the lowest anti-corrosion resistance among the three coatings. According to research conducted by Afroukhteh and Zhang et al. a compact and fine metal-based composite could effectively prevent liquid from penetrating the composite's interior (Ref 42-44). The Ni60-WC20 composite was able to effectively prevent the penetration of the corrosion solution into the coating due to its compact and fine microstructure, thus leading to the outstanding corrosion resistance displayed by the composite.

#### 4. Conclusions

- (1) The WC particles had a substantial effect on the structure of the Ni60-WC composite. The Ni60-WC20 composite had the most meticulous and compact microstructure of the three coatings when compared to the Ni60 composite. Furthermore, the cross-sectional analysis of Ni60-WC10 and Ni60-WC20 composites revealed the presence of numerous elements such as Ni, W, C, Fe, and Cr, confirming the successful application of the LCG approach in Ni60-WC composite prefabrication.
- (2) Diffraction peaks for Ni60 composite were found at  $43.6^\circ$ ,  $50.1^\circ$ , and  $74.7^\circ$ , indicating the presence of only  $\gamma$ -(Ni,Fe) and  $\text{Ni}_3\text{Fe}$  phases. The Ni60-WC20 composite demonstrated an average Vickers hardness of around 826.9 HV, which was roughly 3.5 times more than the Vickers hardness of the substrate, measured at approximately 247.2 HV.
- (3) The Ni60-WC20 composite exhibited exceptional anti-wear properties. The worn surface of the Ni60-WC20 composite exhibited shallow grooves, with a wear depth of approximately  $5.9 \mu\text{m}$ . The corrosion rates of Ni60, Ni60-WC10, and Ni60-WC20 composites were 16.22, 8.39, and 6.33  $\text{mg}/(\text{m}^2\cdot\text{h})$ , respectively. In addition, the corrosion potential of the Ni60-WC20 composite was only  $-0.37 \text{ V}$ , demonstrating its exceptional corrosion resistance.

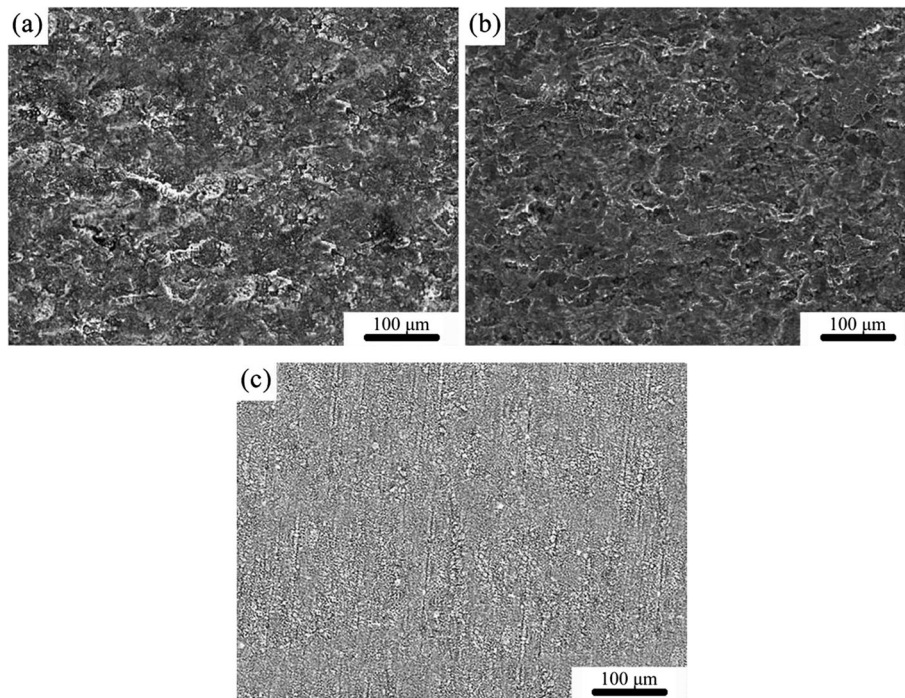


**Fig. 11** SEM images of the corrosion surfaces of (a) Ni60 composite, (b) Ni60-WC10 composite and (c) Ni60-WC20 composite.

## Acknowledgments

The research is supported by National Natural Science Foundation of China (Granted No. 51974089), International Scientific and Technological Cooperation Project (Granted No. GUIQ0700500523) and the Guilin City Science Research and Technology Development Plan Project (Granted No. 20220124-23).

## References

1. L.M. Yao, Z.M. Xiao, A. Ramesh, and Y.M. Zhang, On the Melt Pool Flow and Interlayer Interface Shape in 3D Printing of Dissimilar Alloys, *Int. Commun. Heat Mass Transfer*, 2023, **145**, p 106833
2. C. Zhao, F. Tian, H.R. Peng, and J.Y. Hou, Non-transferred Arc Plasma Cladding of Stellite Ni60 Alloy on Steel, *Surf. Coat. Technol.*, 2002, **155**(1), p 80–84
3. L. Chen, Y. Zhao, X. Chen, T. Yu, and P. Xu, Repair of Spline Shaft by Laser-cladding Coarse TiC Reinforced Ni-based Coating: Process, Microstructure and Properties, *Ceram. Int.*, 2021, **47**, p 30113–30128
4. Y.N. Ma, C.G. Bao, S.C. Song, and J. Lei, Effects of TiC Addition on Microstructures, Mechanical Properties and Fracture Behaviors of Porous Titanium Carbide Ceramics, *Ceram. Int.*, 2018, **44**(16), p 19919–19925
5. P. Farahmand and R. Kovacevic, Corrosion and Wear Behavior of Laser Cladded Ni-WC Coatings, *Surf. Coat. Technol.*, 2015, **276**, p 121–135
6. C. Pan, M. Gong, S. Feng, X. Chen, and P. He, Corrosion and Thermal Fatigue Behaviors of Induction-clad Ni-coated TiC Particle-reinforced Ni60 Coating in Molten Aluminum Alloy, *Surf. Coat. Technol.*, 2021, **419**(9), p 127278
7. J. Lei, C. Shi, S. Zhou, Z. Gu, and L. Zhang, Enhanced Corrosion and Wear Resistance Properties of Carbon Fiber Reinforced Ni-based Composite Coating by Laser Cladding, *Surf. Coat. Technol.*, 2018, **334**, p 274–285
8. C. Shi, J. Lei, S. Zhou, X. Dai, and L. Zhang, Microstructure and Mechanical Properties of Carbon Fibers Strengthened Ni-based Coatings by Laser Cladding: The Effect of Carbon Fiber Contents, *J. Alloy. Compd.*, 2018, **744**, p 146–155
9. J. Huang, Z. Zhu, W. Shi, Y. Zhao, T. Jiao, and K. Li, Microstructure and Properties Analysis of Ni60-based/WC Composite Coatings Prepared by Laser Cladding, *Heliyon*, 2024, **10**(2), p 24494
10. Q. Ma, Y. Li, J. Wang, and K. Liu, Investigation on Cored-eutectic Structure in Ni60/WC Composite Coatings Fabricated by Wide-band Laser Cladding, *J. Alloy. Compd.*, 2015, **645**, p 151–157
11. Q. Wang, Q. Li, L. Zhang, and D. Chen, Microstructure and Properties of Ni-WC Gradient Composite Coating Prepared by Laser Cladding, *Ceram. Int.*, 2022, **48**(6), p 7905–7917
12. Q. Ma, Y. Li, J. Wang, and K. Liu, Microstructure Evolution and Growth Control of Ceramic Particles in Wide-band Laser Clad Ni60/WC Composite Coatings, *Mater. Des.*, 2016, **92**, p 897–905
13. X. Wang, F. Zhou, X. Dai, J. Lei, J. Guo, Z. Gu, and T. Wang, Evaluation and Mechanisms on Heat Damage of WC Particles in Ni60/WC Composite Coatings by Laser Induction Hybrid Cladding, *Int. J. Refract Metal Hard Mater.*, 2017, **64**, p 234–241
14. T. Hatakeyama, K. Sawada, K. Sekido, T. Hara, and K. Kimura, Microstructural Factors of the Complex Creep Rate Change in 18Cr-9Ni-3Cu-Nb-N Steel, *Mater. Sci. Eng. A Struct. Mater. Prop. Microstruct. Process.*, 2022, **831**, p 831
15. A. Inayat, Current Progress of Process Integration for Waste Heat Recovery in Steel and Iron Industries, *Fuel*, 2023, **338**, p 127237
16. R.L.D. Paiva, R.D.S. Ruzzi, and R.B.D. Silva, Contribution to the Selection of Cutting Fluid Type and Its Application Technique for Grinding of Bearing Steel, *Proc. Inst. Mech. Eng. Part B J. Eng. Manuf.*, 2022, **236**(5), p 603–613
17. A.V. Pham, T.H. Fang, V.T. Nguyen, and T.H. Chen, Mechanical Characteristics of Ni50Co50/Ni Substrate During Indentation by Molecular Dynamics, *Modell. Simul. Mater. Sci. Eng.*, 2022, **30**(4), p 045006
18. C.L. Chen, A.X. Feng, Y.C. Wei, Y. Wang, X.M. Pan, and X.Y. Song, Effects of WC Particles on Microstructure and Wear Behavior of Laser Cladding Ni60 Composite Coatings, *Opt. Laser Technol.*, 2023, **163**, p 109425
19. F. Zhang, Y. Qin, T. Hu, A. Clare, Y. Li, and L. Zhang, Microstructures and Mechanical Behavior of Beta-type Ti-25V-15Cr-0.2 Si Titanium Alloy Coating by Laser Cladding, *Mater. Sci. Eng. A*, 2020, **796**, p 140063
20. P. Wu, H.M. Du, X.L. Chen, Z.Q. Li, H.L. Bai, and E.Y. Jiang, Influence of WC Particle Behaviour on the Wear Resistance Properties of Ni-WC Composite Coatings, *Wear*, 2004, **257**, p 142–147



21. W. Li, X. Yang, S. Wang, D. Duan, F. Li, Y. Qiao, Y. Liu, and X. Liu, The Effect of WC Content on the Bonding Strength and Mechanical Properties of WC/Ni60 Coatings of Brake Disc, *Opt. Laser Technol.*, 2022, **149**, p 107822
22. J. Ma, M. Qin, Z. Lin, R. Zhang, and X. Qu, Microstructure and Magnetic Properties of Fe-50%Ni Alloy Fabricated by Powder Injection Molding, *J. Magn. Magn. Mater.*, 2013, **329**, p 24–29
23. N.A. Harbi, K.Y. Benyounis, L. Looney, and J. Stokes, Laser Surface Modification of Ceramic Coating Materials, *Encycl. Smart Mater.*, 2018, **1**, p 445–461
24. X. Zhang, X. Di, W. Jing, X. Zhou, C. Zhang, and C. Li, Effect of Microstructural Evolution on the Mechanical Properties of Intercritical Heat-affected Zone of Quenched-and-Tempered Ultrahigh-Strength Steel, *Steel Res. Int.*, 2022, **8**, p 93
25. S. Zhao, S. Zhou, M. Xie, X. Dai, D. Chen, and L. Zhang, Phase Separation and Enhanced Wear Resistance of Cu88Fe12 Immiscible Coating Prepared by Laser Cladding, *J. Market. Res.*, 2019, **8**(2), p 2001–2010
26. Y. Liu, M. Tang, Q. Hu, Y. Zhang, and L. Zhang, Densification Behavior, Microstructural Evolution, and Mechanical Properties of TiC/AISI420 Stainless Steel Composites Fabricated by Selective Laser Melting, *Mater. Des.*, 2020, **187**, p 103831
27. Q.H. Li, Y.L. Li, Q.F. Bai, C. Chen, C.J. Zhao, and Y.L. Liu, Effect of Power Spinning Combined with Heat Treatment on the Organization and Wear Resistance of High-speed Laser Cladding Coatings, *Mater. Lett.*, 2023, **333**(2), p 133594.1-133594.4
28. W. Li and D. Kong, Effect of Y<sub>2</sub>O<sub>3</sub> Addition on Microstructure and Friction-wear Performances of Laser Cladded CrNi Coatings on AISI H13 Steel, *Ind. Lubr. Tribol.*, 2022, **2**, p 74
29. C. Cui, M. Wu, X. Miao, Z. Zhao, and Y. Gong, Microstructure and Corrosion Behavior of CeO<sub>2</sub>/FeCoNiCrMo High-entropy Alloy Coating Prepared by Laser Cladding, *J. Alloys Compd. Interdiscip. J. Mater. Sci. Solid-state Chem. Phys.*, 2022, **890**, p 161826–161838
30. Y. Liu, X.H. Gu, C.H. Lou, L. Kang, Q.H. Hou, and C.Y. Ma, Influence of WC Ceramic Particles on Structures and Properties of Laser Cladding Ni50-WC Coatings, *J. Market. Res. Res.*, 2023, **26**, p 14–21
31. S.F. Zhou and X.Q. Dai, Dissolution Behavior of Cast WC Particles in NiCrBSi-WC Coatings by Laser Induction Hybrid Cladding, *Adv. Mater. Res.*, 2013, **668**, p 283–287
32. Q.B. Nguyen, Z. Zhu, B.W. Chua, W. Zhou, J. Wei, and S.M.L. Nai, Development of WC-inconel Composites Using Selective Laser Melting, *Arch. Civil Mech. Eng.*, 2018, **18**, p 1410–1420
33. F.Q. Li, X.Y. Feng, and Y.B. Chen, Influence of WC Content on Microstructure of WC/Ni60A Laser Cladding Layer, *Chin. J. Lasers*, 2016, **43**(4), p 117–123
34. L.M. Yao, Z.M. Xiao, S. Huang, and U. Ramamurty, The Formation Mechanism of Metal-ceramic Interlayer Interface During Laser Powder Bed Fusion, *Virtual Phys. Prototyp.*, 2023, **18**(1), p 2235324
35. B. AlMangour, D. Grzesiak, and J. Yang, Nanocrystalline TiC-reinforced H13 Steel Matrix Nanocomposites Fabricated by Selective Laser Melting, *Mater. Des.*, 2016, **96**, p 150–161
36. B. AlMangour, D. Grzesiak, J. Cheng, and Y. Ertas, Thermal Behavior of the Molten Pool, Microstructural Evolution, and Tribological Performance During Selective Laser Melting of TiC/316L Stainless Steel Nanocomposites: Experimental and Simulation Methods, *J. Mater. Process. Technol.*, 2018, **257**, p 288–301
37. F. Deirmina, B. AlMangour, D. Grzesiak, and M. Pellizzari, H13-Partially Stabilized Zirconia Nanocomposites Fabricated by High-energy Mechanical Milling and Selective Laser Melting, *Mater. Des.*, 2018, **146**, p 286–297
38. J.Z. Lu, J. Cao, H.F. Lu, L.Y. Zhang, and K.Y. Luo, Wear Properties and Microstructural Analyses of Fe-based Coatings with Various WC Contents on H13 Die Steel by Laser Cladding, *Surf. Coat. Technol.*, 2019, **369**, p 228–237
39. G. Xie, X. Lin, K. Wang, X. Mo, D. Zhang, and P. Lin, Corrosion Characteristics of Plasma-sprayed Ni-coated WC Coatings Comparison with Different Post-treatment, *Corros. Sci.*, 2007, **49**(2), p 662–671
40. Y. Cui, L. Chen, P. Qin, R. Li, Q. Zang, J. Peng, L. Zhang, S. Lu, L. Wang, and L. Zhang, Metastable Pitting Corrosion Behavior of Laser Powder Bed Fusion Produced Ti-6Al-4V in Hank's Solution, *Corros. Sci.*, 2022, **203**, p 110333
41. P. Qin, Y. Chen, Y. Liu, J. Zhang, L. Chen, Y. Li, X. Zhang, C. Cao, H. Sun, and L. Zhang, Resemblance in Corrosion Behavior of Selective Laser Melted and Traditional Monolithic  $\beta$  Ti-24Nb-4Zr-8Sn Alloy, *ACS Biomater. Sci. Eng.*, 2019, **5**(2), p 1141–1149
42. S. Afroukhteh, C. Dehghanian, and M. Emamy, Preparation of the Ni-P Composite Coating Co-deposited by Nano TiC Particles and Evaluation of It's Corrosion Property, *Appl. Surf. Sci.*, 2012, **258**(7), p 2597–2601
43. D. Zhang and X. Zhang, Laser Cladding of Stainless Steel with Ni-Cr<sub>3</sub>C<sub>2</sub> and Ni-WC for Improving Erosive-corrosive Wear Performance, *Surf. Coat. Technol.*, 2005, **190**(2–3), p 212–217
44. F. Xia, C. Li, C. Ma, Q. Li, and H. Xing, Effect of Pulse Current Density on Microstructure and Wear Property of Ni-TiN Nanocoatings Deposited via Pulse Electrodeposition, *Appl. Surf. Sci.*, 2021, **538**, p 148139

**Publisher's Note** Springer Nature remains neutral with regard to jurisdictional claims in published maps and institutional affiliations.

Springer Nature or its licensor (e.g. a society or other partner) holds exclusive rights to this article under a publishing agreement with the author(s) or other rightsholder(s); author self-archiving of the accepted manuscript version of this article is solely governed by the terms of such publishing agreement and applicable law.